# Evaluating Mesoscale NWP Models Using Kinetic Energy Spectra

WILLIAM C. SKAMAROCK

*National Center for Atmospheric Research,* Boulder, Colorado*

(Manuscript received 16 March 2004, in final form 11 June 2004)

ABSTRACT

Kinetic energy spectra derived from observations in the free atmosphere possess a wavenumber dependence of $k^{-3}$ for large scales, characteristic of 2D turbulence, and transition to a $k^{-5/3}$ dependence in the mesoscale. Kinetic energy spectra computed using mesoscale and experimental near-cloud-scale NWP forecasts from the Weather Research and Forecast (WRF) model are examined, and it is found that the model-derived spectra match the observational spectra well, including the transition. The model spectra decay at the highest resolved wavenumbers compared with observations, indicating energy removal by the model's dissipation mechanisms. This departure from the observed spectra is used to define the model's effective resolution. Various dissipation mechanisms used in NWP models are tested in WRF model simulations to examine the mechanisms' impact on a model's effective resolution. The spinup of the spectra in forecasts is also explored, along with spectra variability in the free atmosphere and in forecasts under different synoptic regimes.

## 1. Introduction

The atmospheric kinetic energy spectra in the free troposphere and lower stratosphere possess a robust and remarkable universality. Results from an observational analysis of kinetic energy spectra, produced in a seminal study by Nastrom and Gage (1985) using the Global Atmospheric Sampling Program (GASP) dataset, are shown in Fig. 1. The spectrum in Fig. 1 illustrates the large-scale $k^{-3}$ dependence of the atmospheric kinetic energy spectrum, along with a transition to a $k^{-5/3}$ dependence found in the mesoscale and smaller scales. Similar behavior over a wide wavenumber range had been previously observed in less comprehensive observational analyses (e.g., Lilly and Peterson 1983; Boer and Shepherd 1983; Vinnichenko 1970). Also depicted in Fig. 1 is the result of an analysis of the Measurement of Ozone and Water Vapor by Airbus In-Service Aircraft (MOZAIC) aircraft observations by Lindborg (1999). Making use of structure functions, Lindborg produced a simple functional fit to the MOZAIC kinetic energy spectrum that results in a remarkably close fit to the GASP kinetic energy spectrum. Additionally, similar results have been reported for kinetic energy (KE) spectra analyses of aircraft data by Cho et al. (1999a,b) for the Pacific Exploratory Missions (PEM) Tropics flights. The results have shown very little dependence on latitude, season, or altitude (Nastrom and Gage 1985; Cho et al. 1999a,b).

The prevailing explanation for the large-scale $k^{-3}$ dependence of the kinetic energy spectrum (between length scales of several thousand to several hundred kilometers) has arisen from applications of 2D turbulence theory (Kraichnan 1967; Lilly 1969; Charney 1971). The theory predicts a downscale enstrophy cascade (and enstrophy inertial range) and no energy cascade in the $k^{-3}$ spectral range below scales of around 5000 km (Boer and Shepherd 1983) where energy is input from the large scale (from differential meridional heating). Examination of global model spectra by Koshyk and Hamilton (2001) and the structure function analyses of Lindborg (1999) and Lindborg and Cho (2001) support the existence of the enstrophy inertial range. Deviations from $k^{-3}$ have typically been argued as arising from the existence of coherent structures.

The mesoscale spectral range is not as well understood. Three-dimensional turbulence theory, which should be appropriate for cloud-scale and below, predicts a $k^{-5/3}$ behavior. This is generally what is observed and found in modeling studies. Three-dimensional turbulence cannot characterize the mesoscale—the flows are highly stratified and 2D in nature. Two explanations for the mesoscale behavior of the spectra have been put forward. One explanation (Gage 1979; Lilly 1983) posits the input of energy at small scales (by convection or other sources) and an upscale transfer (negative cascade) of a small portion of this energy, with the resulting

* The National Center for Atmospheric Research is sponsored by the National Science Foundation.

*Corresponding author address:* William C. Skamarock, National Center for Atmospheric Research, P.O. Box 3000, Boulder, CO 80307-3000.
E-mail: skamaroc@ucar.edu

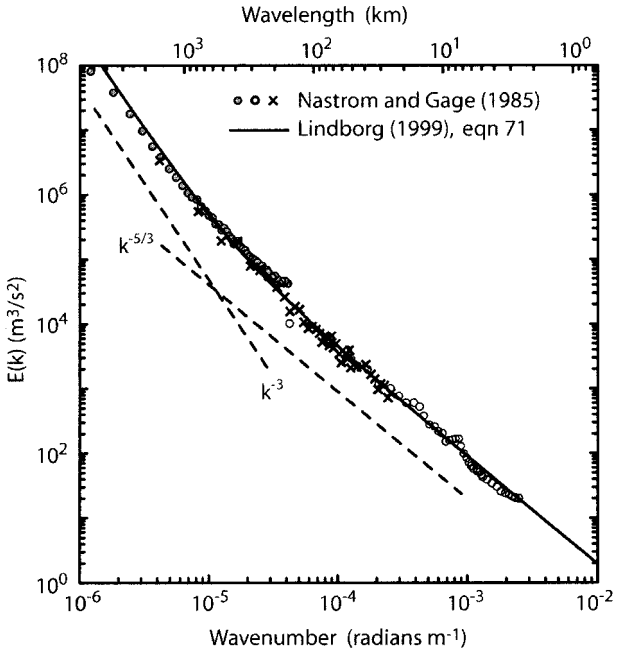


FIG. 1. Nastrom and Gage (1985) spectrum derived from the GASP aircraft observations (symbols) and the Lindborg (1999) functional fit to the MOZAIC aircraft observations.

$k^{-5/3}$ spectrum predicted by stratified (2D) turbulence theory. A second explanation, put forth by Dewan (1979) and VanZandt (1982), suggests that the mesoscale spectrum is dominated by internal gravity waves. The observational analyses of Lindborg (1999) and Lindborg and Cho (2001), using structure functions, do not reveal a negative energy flux in the mesoscale (down to scales of 30 km), rather, a 2D enstrophy inertial range is observed. Below these scales the structure function analyses show that the flow is highly intermittent, and more observations would be needed to conclusively characterize the dynamics of the kinetic energy spectrum. A more detailed description of the 2D theory and observational analyses, including their historical development, can be found in Lindborg (1999).

While the dynamics of the mesoscale portion of the kinetic energy spectrum are not well understood, the spectral characteristics in and of themselves have significant implications for mesoscale and cloud-scale NWP. The $k^{-5/3}$ dependence of mesoscale (and cloud-scale) spectra suggests that the small scales are energetic and that error growth may be faster than at synoptic scales. For mesoscale NWP models with grid sizes $\Delta x$ ranging between 1 and 20 km and forecast periods of 1 to 3 days, many of the resolved features are not predictable and errors at these scales have sufficient time to propagate upscale. Thus the characteristics of the mesoscale kinetic energy spectrum cast doubt on the viability of deterministic small-scale NWP at traditional mesoscale time periods, especially given the additional difficulty of initializing and verifying forecasts at these small scales because of a lack of mesoscale data.

There are a number of reasons, however, to attempt high-resolution mesoscale forecasts. Significant predictability may be possible for small-scale phenomena forced by the large scale (e.g., frontal convection) or tied to fixed forcings such as terrain (e.g., mountain–valley circulations) or surface heterogeneities (e.g., sea breezes). Forecasts may also benefit from improved representation of important small-scale physical phenomena. For example, NWP models using grid spacing smaller than a few kilometers will be able to explicitly resolve deep convection, foregoing the need for a deep convection parameterization. Additionally, nondeterministic products, such as the character of convection in a region during a time period in convective-resolving models, may prove to be valuable forecast aids. Finally, it should be appreciated that at some time in the not-too-distant future we will have the capability to perform ensembles of very high resolution forecasts with the goal of producing statistically meaningful probabilistic forecasts.

With this understanding of the atmospheric spectrum and mesoscale NWP needs and limitations in mind, we examine the ability of a nonhydrostatic mesoscale NWP model [the Weather Research and Forecast (WRF) model; Skamarock et al. 2001; Michalakes et al. 2001] to reproduce observed kinetic energy spectral characteristics. While this is not a traditional validation measure, a model's ability to reproduce observed kinetic energy spectra indicates whether or not it has the correct kinetic energy statistics and, in this sense, if it is faithful to the dynamics of the observed atmosphere.

In examining the WRF model forecasts' kinetic energy spectra, we find that the spectra depart from their expected behaviors at high wavenumbers (short wavelengths) on the model grid. These deviations are a direct measure of an NWP model's true resolution capabilities. We also find that spectra (and a model's true resolution) can be sensitive to the formulation and application of explicit and implicit filters in NWP models. Various filtering mechanisms are examined within the WRF model to understand the character of the different formulations and to serve as a guide to their formulation and tuning.

Model spectra also illustrate the lack of mesoscale observations and assimilation methodologies with which to initialize an NWP forecast model—model spectra are severely deficient in kinetic energy in the mesoscale in forecast initializations. The correct mesoscale spectra, however, develop rapidly in the NWP model forecasts. We examine the initial spinup and adjustment of the mesoscale spectra to verify that physically realistic finescale structures are being generated. High-resolution NWP would be impossible without this spinup, and any analysis of the kinetic energy spectra is dependent on a plausible spinup of the spectrum at the scales that are not initialized.

## 2. Model KE spectra

Global forecast models and climate models generally reproduce the large-scale $k^{-3}$ spectral character, and the spectra are regularly used to examine filter formulations (e.g., Laursen and Eliasen 1989). As the resolution of the global models has increased, global model spectra are being examined to see if they capture the transition to the $k^{-5/3}$ mesoscale behavior. For example, Koshyk and Hamilton (2001) find evidence of this transition in the Geophysical Fluid Dynamics Laboratory (GFDL) SKYHI general circulation model that has a nominal resolution of 30 km, but they note that there may be problems with the model dissipation given the strongly upturned spectral tails.

At small scales, cloud model simulations of convection have been evaluated using kinetic energy spectra. Convective simulations clearly show a $k^{-5/3}$ spectral dependence (e.g., Vallis et al. 1997; Lilly et al. 1998), in addition to showing that the kinetic energy is dominated by the kinetic energy associated with divergent modes, as opposed to the dominance of the rotational energy at the large scales. The spectra have also been used to estimate the resolution capabilities in some idealized cases (Bryan et al. 2003). Additionally, vertical velocity spectra have been used in a case study by Lean and Clark (2003) to estimate resolution capabilities of a high-resolution NWP model.

In contrast to global models and cloud models, the kinetic energy spectra of mesoscale NWP models have not been examined in any detail, most likely because a number of difficulties arise in computing and evaluating spectra from limited area forecasts. First, there is the difficulty of computing spectra in nonperiodic domains. A number of approaches have been developed to overcome these problems (e.g., Errico 1985; Denis et al. 2002) and we outline our approach in the appendix. Second, atmospheric spectra have typically been time-averaged over long periods, often over seasons in climate and global models, in order to filter noise from the signal and to overcome problems associated with truncation. As will be shown shortly, long averaging periods do not appear to be necessary for filtering transients and we are able to produce stable spectra averaging over a single diurnal period. Third, there is no data to directly verify the spectra as a component of an NWP forecast, hence the value of the spectra is not obvious. We will demonstrate, however, that KE spectra can be used to examine model damping and effective model resolution. Finally, spectra can vary because of synoptic conditions and the geographic regions of the forecasts. Examples will illustrate these influences.

### *a. Spectra from the WRF Model*

In the Bow Echo and Mesoscale Convective Vortex Experiment (BAMEX) field campaign (Davis et al. 2004) that occurred between mid-May and early July 2003, the WRF mass-coordinate model was used to produce daily 36-h forecasts using grids with horizontal grid spacing of 22, 10, and 4 km beginning at 0000 UTC each day (there were also 1200 UTC forecasts that we do not examine here). The forecast domains were centered over the central United States and the model configurations are described in Done et al. (2004). The late-spring/early-summer BAMEX period was convectively active, with an average of two to three long-lived convective systems occurring within the field program (and forecast) domain per day (Done et al. 2004, manuscript submitted to *Atmos. Sci. Lett.*). There were generally some weak-to-moderate synoptic-scale waves traversing the region, most often in the northern or central latitudes of the forecast domains.

Kinetic energy spectra for the BAMEX forecasts are computed using a one-dimensional spectral decomposition of the velocities ($u$, $v$, $w$) along west–east horizontal grid lines spanning the domain. The energy densities are time averaged over a 24-h period, typically at 3-h intervals. We usually begin the time-averaging at least 12 h into a forecast in order to avoid model spinup issues. Additionally, the energy densities are spatially averaged, both horizontally and vertically. With respect to the horizontal averaging, the energy densities from the west–east grid lines are averaged over the south–north extent of the domain. We do not use velocities from the outer (lateral) 15 points at the start and end of a west–east grid line, and we spatially average energy densities from lines beginning 15 points from the southern boundary and ending 15 points from the northern boundary; this should minimize the effects of the lateral boundary conditions. With respect to the vertical averaging, most spectra are computed on horizontal model surfaces located between 3 to 9 km above sea level (the free troposphere), and are averaged over these surfaces. We have also computed spectra on constant pressure surfaces and on constant height surfaces and found that there is little significant difference among these spectra. On a typical WRF BAMEX grid, the computation of the final spectrum uses an average of more than 20 000 individual 1D spectra (from the west–east grid lines). In comparison, the most comprehensive observational spectra, from GASP (Nastrom and Gage 1985) and MOZAIC (Lindborg 1999) were produced using approximately 5000 flights each. Further information on the spectral computations can be found in the appendix.

We have computed kinetic energy spectra from the 4-km BAMEX forecasts for the entire forecast period (daily 36-h forecasts initialized at 0000 UTC from 5 May 2003 through 14 July 2003). Figure 2 shows the time-averaged spectrum and its standard deviation for this forecast period along with the Lindborg (1999) functional fit to the MOZAIC spectrum. The 4-km forecast spectrum follows the Lindborg spectrum very well, indicating that the forecast spectrum follows the MOZAIC observations and the GASP observations of Nastrom and Gage (1985) shown in Fig. 1. The forecast

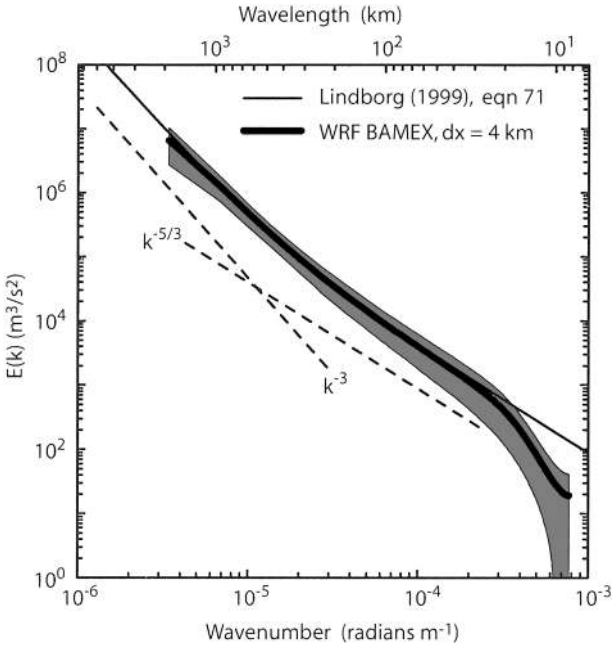


FIG. 2. Spectra from the 4-km WRF BAMEX forecasts from 5 May to 14 Jul 2003. The shaded area encloses plus/minus one std dev. The Lindborg (1999) functional fit to the MOZAIC aircraft observations is also plotted.

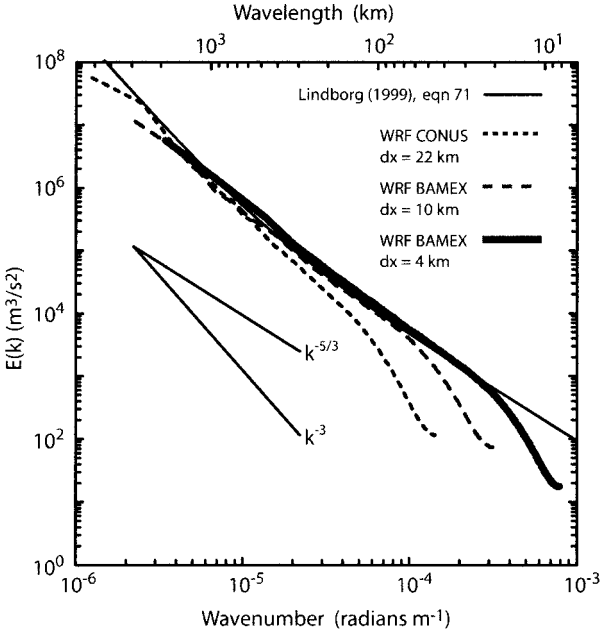


FIG. 3. Spectra computed from WRF BAMEX forecasts initialized at 0000 UTC on 1, 2, and 3 Jun 2003 for 22-, 10-, and 4-km forecast grids. The Lindborg (1999) functional fit to the MOZAIC aircraft observations is also plotted.

spectrum has a slope of somewhat less than −3 at large wavelength and transitions to a shallower slope with increasing wavenumber, following the Lindborg (1999) spectrum function down to wavelengths around 30 km. There is significant variance associated with this spectrum as revealed by the magnitude of the standard deviation relative to the energy density depicted in Fig. 2. The standard deviation is similar in magnitude to the energy density for all wavelengths. This is consistent with the GASP observations as suggested by the spread in the GASP observational spectrum plotted in Fig. 1.

For more detailed study, we have chosen to examine spectra from 4-, 10-, and 22-km forecasts initialized at 0000 UTC on 1, 2, and 3 June 2003; these spectra are from a typical BAMEX weather regime. Figure 3 is a plot of the forecast spectra averaged over the 3-day period. Similar to the 4-km spectrum shown in Fig. 2, these forecast spectra show energy levels that are generally of the correct magnitude overall except at the highest wavenumbers, where model dissipation removes energy and depresses the spectra. The 22-km Contiguous United States (CONUS) forecast shows a small indication of a transition in spectral slope from −3 to a shallower slope, while both the 10- and 4-km forecast spectra show clear evidence of the shallower mesoscale regime but little of the $k^{-3}$ regime. The KE spectra for the 10- and 4-km forecasts possess slopes of approximately −2 in the mesoscale, close to the Nastrom and Gage (1985) analysis, similar to the Lindborg (1999) functional fit to the MOZAIC data (Fig. 1) and consistent with observations from the Pacific Exploratory Missions (PEM) in the 1990s (Cho et al. 1999a,b).

As noted earlier, the Nastrom and Gage spectrum was computed from flight-level aircraft observations whereas the forecast spectra shown in Fig. 3 are averaged over the free troposphere. Figure 4 shows the model spectra

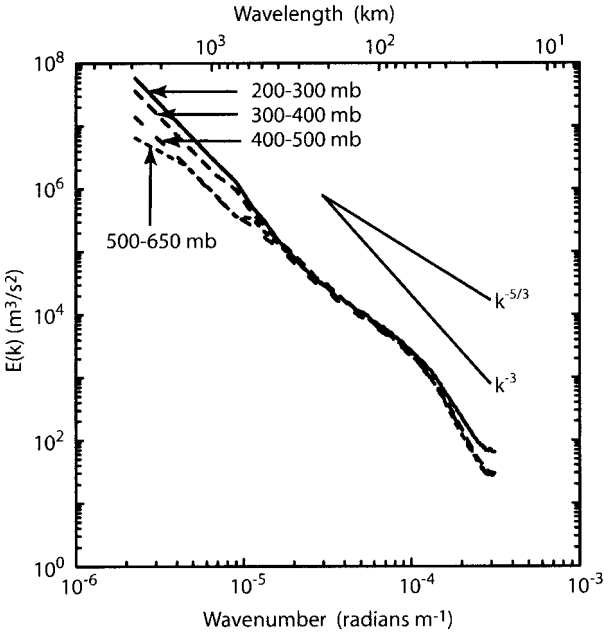


FIG. 4. Spectra from the 1 Jun 2003 BAMEX 10-km forecast averaged between various pressure levels.

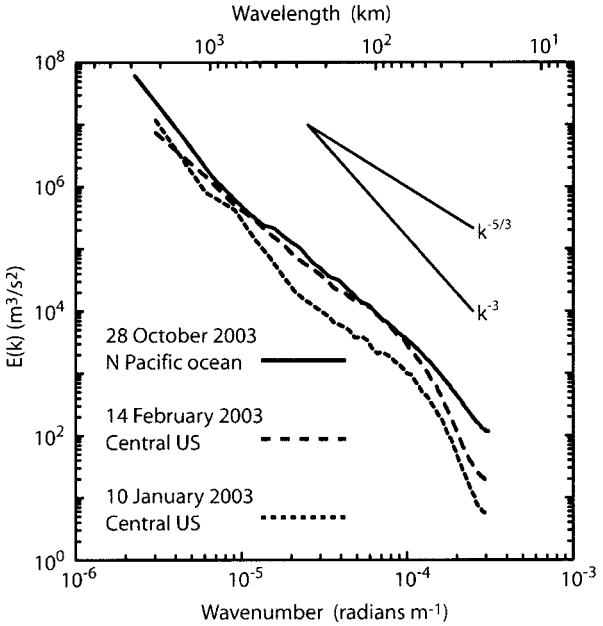


FIG. 5. Spectra from winter forecasts over the central United States, and an autumn forecast over the north-central Pacific Ocean.

from the 10-km forecasts vertically averaged between different model pressure levels (where the velocity fields have been interpolated to constant pressure surfaces before the spectral decomposition). The pressure levels between 150 and 300 hPa roughly bound the majority of flight levels over which the Nastrom and Gage spectrum was computed. The pressure-level spectra are very similar to the tropospherically averaged spectra with the only significant difference being that the energy at the longer wavelengths is greater in the upper levels of the atmosphere. This may arise from the existence of synoptic- and planetary-scale waves in the upper troposphere. More importantly, the model forecast spectra (both the tropospheric averages and that averaged between various pressure levels in the free atmosphere) show the same general character as the Nastrom and Gage spectrum, providing further evidence for the universality of the spectral character and providing evidence that the tropospheric averages are appropriate characterizations of the mesoscale spectra throughout the troposphere and lower stratosphere.

The spread of the forecast spectra shown in Fig. 2 indicates that spectra at individual times can vary significantly from the time-averaged mean. Closer examination of the forecast spectra reveal that the spectral character of NWP forecasts can vary significantly with different synoptic regimes and forecast domain locations. Spectra for three different forecasts using 10-km grids in the WRF-mass model are presented in Fig. 5. The first two forecast domains are centered over the central United States and were initialized 0000 UTC 10 January 2003 and 0000 UTC 14 February 2003, and the third forecast domain was centered over the north-central Pacific Ocean and was initialized 0000 UTC 28 October 2003. The kinetic energy spectra for the January and February forecasts differ substantially in that there is significantly less kinetic energy in the mesoscale portion of the spectrum in the earlier forecast. Figure 6 shows plots of forecast surface pressure, 500-hPa heights, and 3-h rainfall accumulation at times during which spectra were computed from the forecasts. The 10 January forecast is dominated by a large ridge and a surface high with no significant precipitation, and there is little discernable mesoscale structure over most

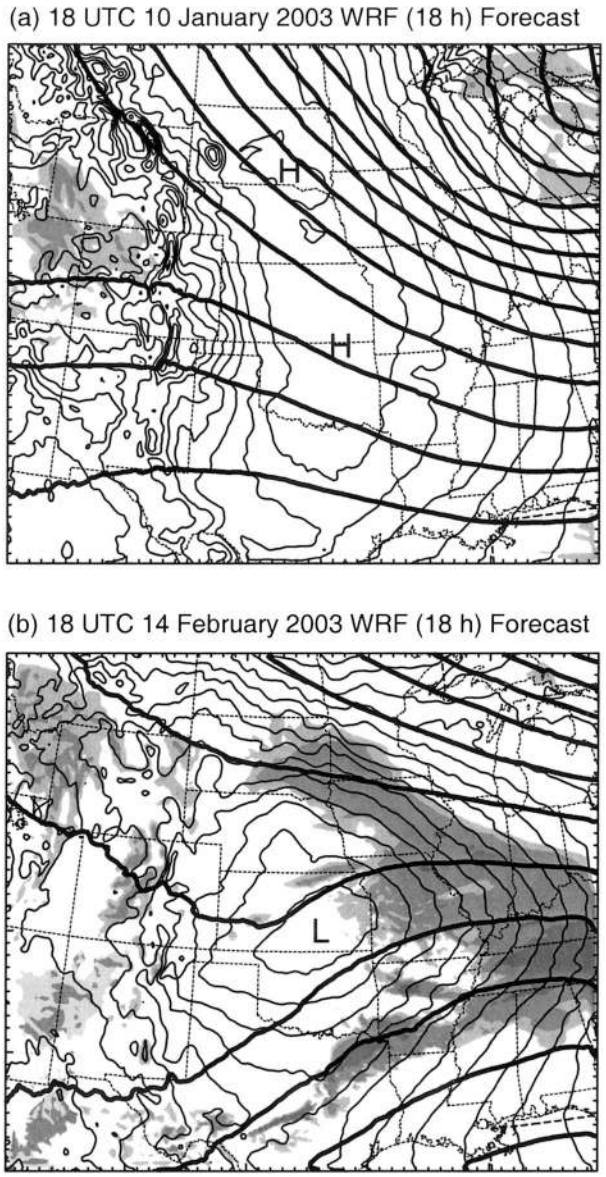


FIG. 6. The 18-h forecasts from a 10-km WRF model configuration over the central United States for 1800 UTC 10 Jan and 14 Feb 2003. Surface pressure is contoured using the thin lines with a 2-hPa contour interval, 500-hPa heights are contoured using the thick lines with a contour interval of 60 m, and 3-h accumulated rainfall is shaded at 0.1, 2, and 5 mm (light to dark).

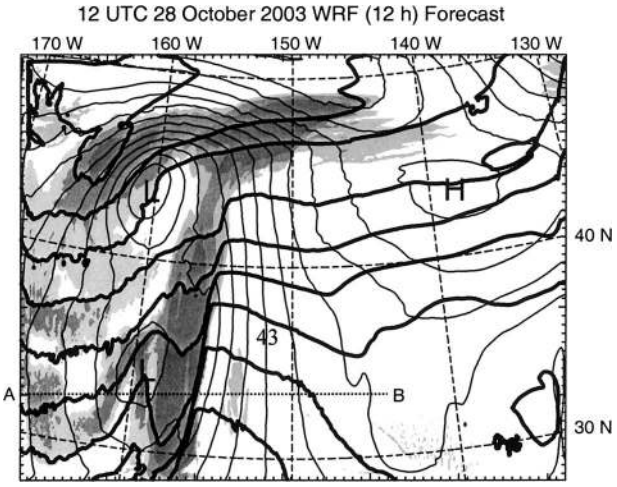


FIG. 7. The 12-h forecast from a 10-km WRF model configuration over the north-central Pacific for 1200 UTC 28 Oct 2003. Surface pressure is contoured using the thin lines and a 2-hPa contour interval, temperature is contoured using the thick lines with a contour interval of 2°C, and 3-h accumulated rainfall is shaded at 0.1, 2, and 5 mm (light to dark).

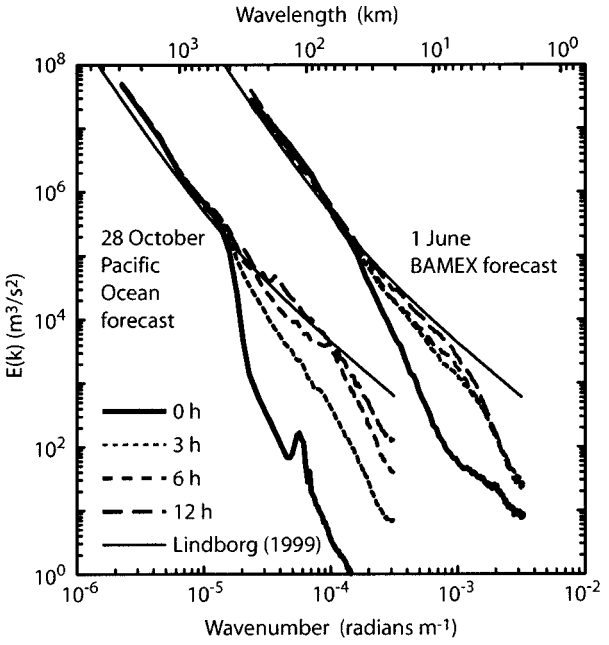


FIG. 8. Spinup of (left) the WRF model spectra for the autumn forecast over the north-central Pacific Ocean and (right) the 1 June BAMEX forecast. The Pacific forecast is initialized from an 80-km Global Forecast System (GFS) analysis, and the BAMEX forecast is initialized with a 40-km Eta analysis. The BAMEX forecast spectra are shifted one decade to the right for clarity.

of the forecast domain. The 14 February forecast, in contrast, contains an extratropical cyclone in the center of the forecast domain and significant mesoscale structure as indicated in the precipitation fields and surface pressure. The difference in mesoscale kinetic energy implied in these forecasts is confirmed in the spectra depicted in Fig. 5. Of the three forecast spectra in Fig. 5, that from the north-central Pacific forecast is perhaps the closest to the climatological spectra in Fig. 1. The oceanic forecast shows a clear $k^{-3}$ range at large scales, which is consistent with the strong oceanic extratropical cyclone found in the forecast and depicted in Fig. 7. The $k^{-3}$ range is somewhat more ambiguous in the winter continental cases.

We have examined spectra from a number of other model forecasts using different resolution, domains, and forecast locations. Overall, the general behavior of the forecast spectra follow the Nastrom and Gage climatology. Variations are found that are similar to those depicted earlier. Additionally, as the physical domain size decreases, physical features can lead to pronounced signatures in the spectra, such as local spectral peaks at the scale of the dominant topographic features.

### *b. Model generation of the mesoscale spectrum*

As has been shown, the WRF-mass model forecast spectra are generally similar to the climatologically observed spectra over the spatial scales that the model can be expected to simulate accurately, with allowance for synoptic regimes and geographical influences. This is consistent with our understanding that a forecast model can be expected generally to resolve features with wavelengths as small as 6–10 $\Delta x$ up to wavelengths as long as the domain. This fully developed KE spectrum is not, however, characteristic of the initial states of high-resolution NWP model forecasts. Initial states for NWP forecasts are smooth because the analyses are smooth—observations to initialize the fine scales are not generally available and data assimilation methods that can use high-resolution observations are not yet mature. Given that forecast models must, of necessity, develop the mesoscale KE spectrum on their own, two questions arise: 1) Is the time scale of the development consistent with our theoretical understanding of KE energy inputs into the atmosphere and of the KE spectrum and its evolution? and 2) Are the mesoscale phenomena that develop in this early time period dynamically consistent with mesoscale phenomena as we observe them?

To address these questions, consider the WRF-mass model forecast KE spectra, shown in Fig. 8, for the 1 June BAMEX forecast on the 10-km grid at 0, 3, 6, and 12 h. At the initial time there is very little energy in the KE spectra at the mesoscale and below, as expected (the WRF-mass model is initialized from a 40-km Eta Model analysis). Figure 8 also shows that the mesoscale portion of the KE spectrum, missing at the initial time, develops rapidly and reaches a fully developed state somewhere between 6 to 12 h into the forecast. Development of the KE spectrum for the 28 October forecast over the ocean is also plotted in Fig. 8 and shows a similarly rapid development.

Energy can appear in the mesoscale portion of the

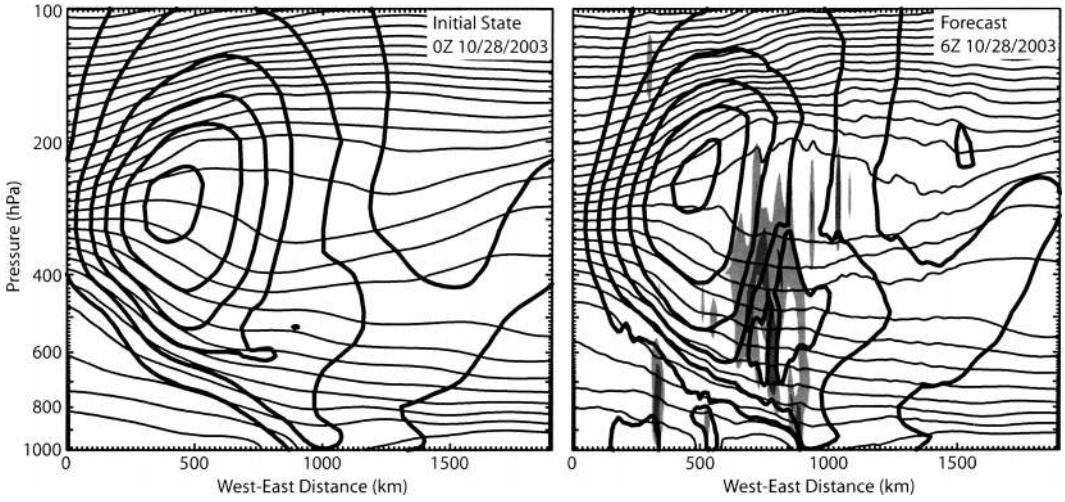


FIG. 9. Nominally west–east cross sections from the 28 Oct 2003 WRF north-central Pacific forecast along the line AB in Fig. 7. The $v$ horizontal velocity (nominally south–north) is contoured using thick lines and a contour interval of 10 m $s^{-1}$, potential temperature is contoured using thin lines and a contour interval of 4 K, and vertical velocity is shaded at 10 and 20 cm $s^{-1}$.

spectrum by three processes—direct forcing (flow interaction with topography, convection, etc.), downscale cascade from longer wavelengths, and upscale cascade from smaller wavelengths. Yuan and Hamilton (1994), in an analytic and modeling study using the 2D shallow-water equations, found that there is a broadband interaction between modes in the energy cascade associated with the transfer of energy between divergent modes; the inertia-gravity modes in each spectral band in the shallow-water system gain energy from all modes of larger scale and lose energy to all modes of smaller scale. This result suggests that energy input from the larger scale (the resolved scales in the initial analyses) should quickly fill the mesoscale kinetic energy spectrum which is dominated by divergent motions. Additionally, energy input in the mesoscale portion of the spectrum should quickly cascade through the entire mesoscale (divergent) portion of the spectrum. The time scales for this energy cascade are typically observed to be something less than an eddy turnover time which, for length scales of a few hundred kilometers or less, should be significantly less than a day. Time scales will be even shorter for the upscale cascade from the smaller mesoscale and cloud-scale motions that are externally and internally forced (e.g., mountain waves and convection, respectively). Terrain forcing can also input energy directly into the mesoscale throughout the mesoscale spectrum, because the terrain possesses structure on all scales. Perhaps not coincidentally, the earth's topography possesses a power spectrum that follows a $k^{-2}$ behavior (e.g., Balmino 1993).

From a phenomenological perspective, a variety of structures appears over the first few hours of the BAMEX high-resolution forecasts. If the forcing mechanisms are in place, convection and convective systems appear within the first few hours. Surface and upper-level fronts collapse to the resolution of the grid (e.g., the surface front in Fig. 7) and finescale flow structure, including gravity waves (Snyder et al. 1993), develop as the large-scale flow encounters the fronts (cf. Figs. 9a and 9b) and topographic features. The finescale structures that develop in the spinup period appear physically realistic and dynamically consistent with our understanding of the atmosphere.

The spinup period for the mesoscale spectrum and the accompanying mesoscale structure is short (hours) relative to typical mesoscale NWP forecast periods (days). With respect to high-resolution NWP, this rapid spinup of mesoscale structure is crucial because the mesoscale portion of the spectrum cannot be initialized given the lack of mesoscale observations and assimilation capabilities. Additionally, the relatively rapid spinup implies that high-resolution NWP forecasts may have increased value because they may be able to deterministically predict mesoscale structure if correctly forced by the larger scale or by external forcings (e.g., deep convection forced by fronts), or they may remove the need for problematic parameterizations (e.g., parameterizations of deep convection).

## 3. The effective resolution of NWP models

Worldwide, NWP continues to move to increasingly higher-resolution forecasts. This evolution is primarily driven not by the need to better resolve features already well resolved in existing high-resolution NWP forecasts, rather it is being driven by the desire to resolve those phenomena that are now marginally resolved, such as convective systems, or currently unresolved and hence parameterized, such as individual convective cells.

The evolution to increasing resolution in NWP forecasts is costly; doubling the horizontal grid density typ-

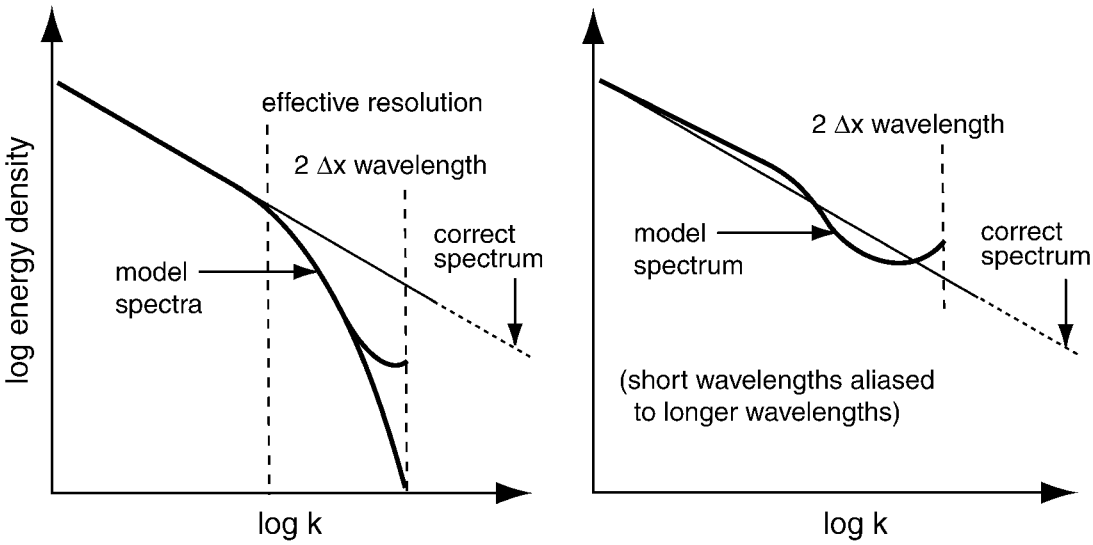


FIG. 10. Schematic depicting the possible behavior of spectral tails derived from model forecasts. Using the methodology outlined in the appendix to compute the spectra, limited-area models (including WRF) usually produce the slightly upturned tail shown at left.

ically increases the integration cost by a factor of 8. Thus a major goal in the development of any NWP model is to maximize model efficiency, where efficiency is defined as the accuracy of the solution relative to the cost of the numerical integration. With respect to the goals of high-resolution NWP, a critically important measure of an NWP model's accuracy is its ability to resolve features at the limits of its grid resolution. Spectra, by providing an integrated measure of the solution energy (i.e., variance) as a function of scale, can be examined to determine the resolution limits of an NWP model in a relatively unambiguous manner.

As discussed in section 2, mesoscale NWP models can and should reproduce the observed features of the atmospheric kinetic energy spectrum. A model's ability to resolve the spectrum at increasingly higher wavenumbers will be limited by the grid size, the integration techniques employed in the model, and the dissipation mechanisms used in the model including both explicit and implicit mechanisms inherent in the chosen integration scheme. The need for dissipation is unavoidable since the downscale energy cascade requires a removal of energy at the highest wavenumbers to prevent an unphysical buildup of energy. The dissipation mechanisms will necessarily be somewhat ad hoc in mesoscale and cloud-scale NWP models because there is no theory to guide the formulations until we reach large-eddy simulation (LES) resolutions of a few hundred meters or less. Even with this lack of theoretical guidance, an NWP model's kinetic energy spectrum can be directly examined to determine the effectiveness of a model's formulation and its dissipation mechanisms.

### *a. Effective resolution*

The most revealing feature of model KE spectrum are the tails, that is, the high-wavenumber portion of the spectrum. Examples of model spectra from the literature and in this paper suggest that four general types of model behavior exist, and three of these are depicted schematically in Fig. 10 [the fourth, where the model spectrum matches the observed spectrum down to the model truncation, can be obtained with some spectral large eddy simulation (LES) models for some cases, e.g., Otte and Wyngaard (2001); these formulations are not valid at NWP model resolutions nor are they general]. The first two types show the energy density decaying as the grid resolution limit is reached (the left panel in Fig. 10). Model filters remove energy most strongly at the highest wavenumbers, with less energy removal occurring at decreasing wavenumbers (increasing wavelengths). Given that model discretizations typically produce their greatest errors at the smallest wavelengths, the small amount of energy in these modes (relative to what would exist at these wavenumbers) means that there is little energy to be aliased to the longer, well resolved modes. The 1D spectra we have computed on spatially limited domains tend to have a small upturn at the end of the tails, as opposed to the steep decay shown in LES-derived spectra or spectra from global models (e.g., Laursen and Eliasen 1989; Koshyk and Hamilton 2001).

The right panel in Fig. 10 shows a spectrum where the highest wavenumber modes in an NWP model are poorly handled—there is buildup of energy to physically unrealistic levels at the highest wavenumbers. Energy is being reflected (aliased) to the lower wavenumber modes of the solution and the reflection casts doubt on a considerable portion of the spectrum and the physical phenomena represented by these modes.

The WRF model spectra presented in section 2 possess spectral tails corresponding to the left panel in Fig.

10, that is, the WRF model spectral tails are damped and decaying relative to the actual spectra. These results represent our best attempt at a minimal-dissipation configuration of the model. Further reduction of the dissipation in the WRF model would lead to increased energy at the smaller scales and better spectral tails. When we attempt to do this, however, we see structures at the grid scale that appear physically unrealistic. From a theoretical perspective, the normalized group velocities of the shorter wavelength modes ($2\Delta x$ to $4\Delta x$) in finite-difference models are often zero or even negative. Thus the unphysical behavior of the highest wavenumber modes suggest that aliasing and phase errors will be a problem—as we observe in the solutions where we decrease the dissipation beyond our minimal-dissipation configuration. Damping of the highest wavenumber modes, producing spectra such as that shown in the left panel in Fig. 10, is therefore prudent.

Model spectra also reveal important information concerning resolved and underresolved modes in a simulation. We can define the effective resolution of a model as the wavelength where a model's spectrum begins to decay relative to the observed spectrum or relative to a spectrum from a higher-resolution simulation (that should resolve higher wavenumbers before numerical dissipation leads to decay). The rationale behind this definition is that modes with wavenumbers higher than the effective resolution (modes with shorter wavelengths) are damped relative to their atmospheric counterparts and hence are dynamically suspect. This effective resolution is depicted in the schematic Fig. 10a.

For the WRF BAMEX simulations, Fig. 11 reveals that the effective resolution of the WRF model 22-, 10-, and 4-km configurations, using the 1–3 June forecast spectra (given in Fig. 3), is generally around $7\Delta x$. The fact that the effective resolution of the WRF model is a constant multiple of $\Delta x$ is not surprising because the model filters scale with the model grid spacing. Given the problems with phase errors for increasingly shorter wavelengths, we believe that we are close to the limit of the spatial resolving capabilities of finite-difference models that use explicit methods.

In examining the WRF forecasts we have used the functional fit to the MOZAIC observational spectrum given by Lindborg (1999) as a reference in Fig. 11. Both the 10- and 4-km WRF forecast spectra closely parallel the Lindborg analysis, and differences in energy levels between the two forecast spectra are likely the result of differences in the horizontal extent of the domains. This situation is somewhat fortuitous given that we have noted, in section 2, that the forecast spectra can be influenced by the synoptic regime and the geographical region. Alternatively, we could have used the 4-km forecast spectrum to determine the effective resolution of the 10-km forecast. Determining the effective resolution of the 22-km forecast presents other difficulties. The 22-km forecast spectrum has a slightly steeper slope than the Lindborg analysis (and the 10-

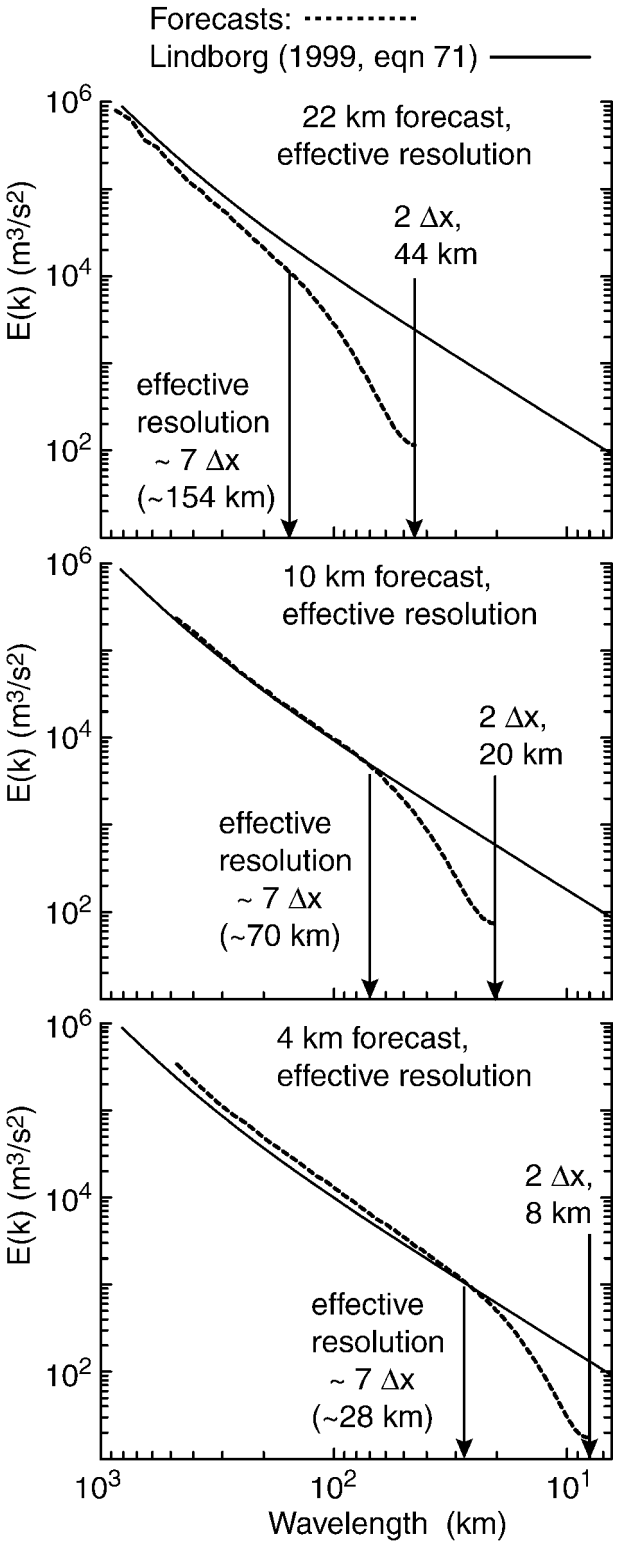


FIG. 11. Effective resolution determined from forecast-derived spectra for the BAMEX-configured WRF model at 22-, 10-, and 4-km horizontal grid spacing. The model forecast spectra are those plotted in Fig. 3.

and 4-km forecast spectra) for wavelengths much below 500 km. The reason for this difference is that the 22-km forecast uses a domain that is much larger than the 10- and 4-km domains (e.g., it extends well beyond the continental United States in all directions compared with the 10-km domain) and it also possesses regions where the flow is not as energetic as that in the central United States in this time period. Here we look closely at where the spectral slope begins to steepen with higher wavenumber in the log-log plots, as opposed to becoming shallower as indicated by the observational spectrum, to determine the effective resolution.

### *b. NWP model dissipation*

Within the WRF model, many dissipation formulations used in NWP models have been implemented and tested using the forecasts presented in section 2. These formulations include the implicit dissipation formulations inherent in upwind-biased advection schemes (i.e., the standard WRF formulation), second-order and fourth-order filters using an eddy viscosity or higher-order damping term of the form

$$\frac{\partial \phi}{\partial t} = \cdots + \nu_2 \frac{\partial^2 \phi}{\partial x^2}; \tag{1a}$$

$$\cdots - \nu_4 \frac{\partial^4 \phi}{\partial x_i^4}, \tag{1b}$$

where $\phi$ represents the model prognostic variables, second- and fourth-order filters scaled by some function of the horizontal deformation $F$,

$$\frac{\partial \phi}{\partial t} = \cdots + F\nu_2 \frac{\partial^2 \phi}{\partial x_i^2}; \tag{2a}$$

$$\cdots - F\nu_4 \frac{\partial^4 \phi}{\partial x_i^4}, \tag{2b}$$

and horizontal divergence damping

$$\frac{\partial u_i}{\partial t} = \cdots + \nu_d \frac{\partial}{\partial x_i} \nabla_h \cdot \mathbf{V}. \tag{3}$$

To illustrate the effects these filters have on spectra, we have produced forecast spectra for the 1 June 2003 BAMEX case using the 10-km WRF-BAMEX configuration and the filters (1a), (1b) and (3) along with commonly used values for the viscosities and hyperviscosities. In these tests we have used second-order centered advection operators as opposed to the upwind-biased operators used in the reference forecast. Figure 12 depicts the spectra resulting from these computations, and the following observations can be drawn from them:

1) The reference spectrum (plotted in both Figs. 12a and 12b), produced using fifth-order upwind advection (that contains a sixth-order filter with a hyperviscosity proportional to the advective Courant number; see Wicker and Skamarock 2002), is the minimally dissipative member of the set and the most scale selective. Scale selectivity in this case refers to a filter's selective damping of higher-wavenumber modes.
2) The fourth-order horizontal filter [Eq. (1b), Fig. 12a] produces results similar to the fifth-order upwind advection, but is slightly less scale selective. Increasing

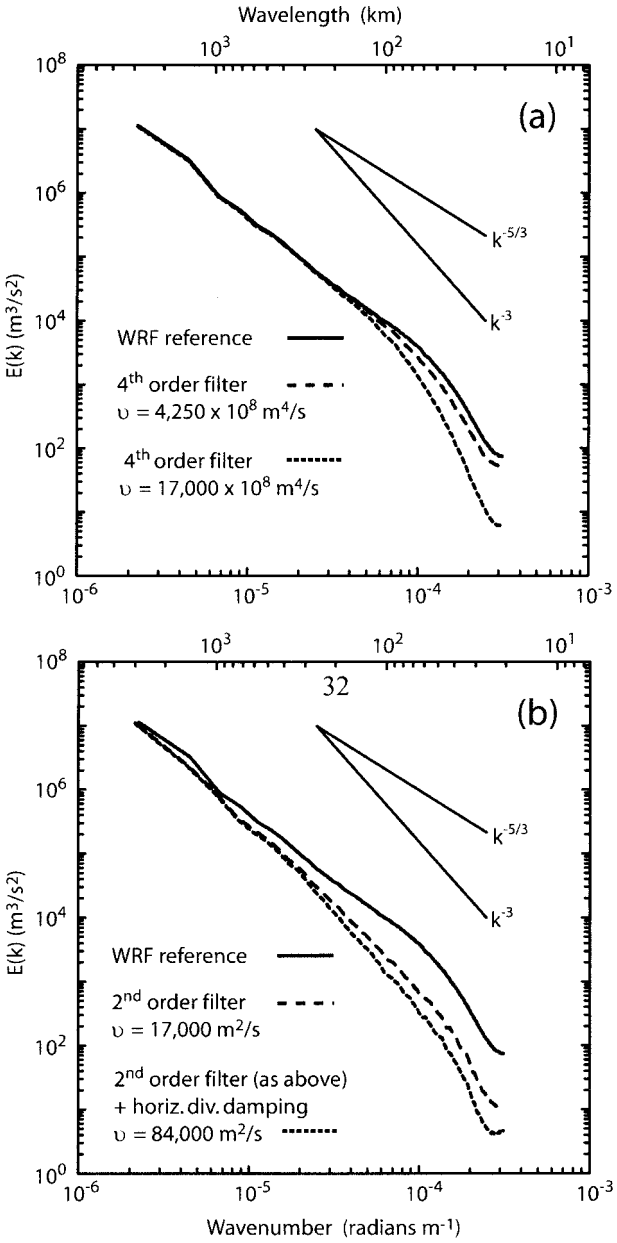


FIG. 12. Spectra computed from WRF model forecasts with 10-km grid spacing using various filter formulations. (a) Results using a fourth-order filter with two different hyperviscosity values. (b) Results when using a second-order filter with a hyperviscosity chosen to damp 2 $\Delta x$ modes at the same rate as the fourth-order filter results in (a) (cf. the same line types). Horizontal divergence damping, added to the horizontal second-order filter, produces the most severely damped spectra, as shown in (b).

the hyperviscosity results in lower effective resolution compared with the upwind advection results. The two values used in producing the spectra in Fig. 12a roughly bound the values used in NWP models such as Advanced Regional Prediction System (ARPS; Xue et al. 2003), Coupled Ocean–Atmosphere Mesoscale Prediction System (COAMPS; Hodur 1997), fifth-generation PSU–NCAR mesoscale model [MM5; that scales the hyperviscosity (2b) but has a lower bound; Dudhia 1993] and other models using the fourth-order filter formulation.

3) The second-order filter with a fixed eddy viscosity [Eq. (1a), Fig. 12b] is much less scale selective than its fourth-order counterpart. The second-order filter with an eddy viscosity of 17 000 $m^2\ s^{-1}$ damps the $2\Delta x$ modes at the same rate as the fourth-order filter with a hyperviscosity of $4250 \times 10^8\ m^4\ s^{-1}$. Comparison of these two results also shows that the energy at the highest wavenumbers is much less when using the second-order filter even though the damping rate on the $2\Delta x$ modes is the same. The second-order filter, being much less scale selective, removes a significant amount of energy at the lower wavenumbers; hence there is less energy to cascade downscale. The value of 17 000 $m^2\ s^{-1}$ is the lower bound on the deformation-scaled second-order damping (2a) used in the National Centers for Environmental Prediction (NCEP) Nonhydrostatic Mesoscale Model (NMM) model (Janjic 2003) at 8-km horizontal grid spacing.
4) Horizontal divergence damping [Eq. (3), Fig. 12b] preferentially damps the spectrum in the mesoscale where the kinetic energy is largely contained in divergent motions. The viscosity used in this test of the filter is 84 000 $m^2\ s^{-1}$, the nominal value used in the NCEP NMM model at 8-km horizontal grid spacing.

As noted previously, the spectra in these 10-km WRF forecasts were best captured using the sixth-order Courant number–dependent filter implicit in the upwind-biased advection. Even more scale-selective higher-order filters could be used. Yuan and Hamilton (1994), examining the spectra produced in a forced-dissipative $f$-plane shallow-water system, found that the nonlinear interactions among the inertia-gravity waves is very broadband in spectral space. They state that this argues for a nonlinear flow-dependent dissipation formulation. For NWP models, this suggests that the effectiveness of higher-order filters needs to be carefully evaluated, and that moving to filters of very high order (e.g., greater than sixth order) may not be advantageous.

## 4. Summary and discussion

Kinetic energy spectra from mesoscale NWP forecasts (WRF model, 22- and 10-km grid lengths) and near-cloud-scale NWP forecasts (WRF model, 4-km grid lengths) have been examined, and the results can be summarized as follows:

1) The forecast spectra are found to be similar to the observationally derived spectra of Nastrom and Gage (1985), Lindborg (1999), and Cho et al. (1999a,b). The forecast spectra reproduce the observed $k^{-5/3}$ wavenumber dependence characteristic of the mesoscale, and its transition from a steeper $k^{-3}$ behavior at the larger scales.
2) The forecast spectra are robust with only a small dependence on altitude from the lower free troposphere up to the lower stratosphere, along with some sensitivity to synoptic conditions and geography.
3) The initial conditions for the forecasts, taken from smooth analyses, possess little mesoscale energy (energy in wavelengths less than approximately 300 km). The development of the mesoscale portion of the spectrum takes 6 to 12 h, a time scale consistent with theory and with the development of finescale structures in the forecasts.
4) The effective resolution of a model can be defined as the scale at which the model spectrum decays relative to the expected spectrum. Model spectra, and effective resolution, can be affected by model damping, and the scale of the finest resolvable modes (the resolving power of the model) is strongly dependent on the formulation and tuning of implicit and explicit model filters. NWP model filters that are not scale selective can deleteriously damp the spectrum at low wavenumbers.

These results are encouraging for high-resolution NWP forecasting (that is, model forecasts produced using mesoscale to cloud-resolving spatial resolutions). Specifically, high-resolution NWP models generally produce dynamically consistent finescale structure and produce the climatologically appropriate energy spectrum. Moreover, structures (and energy) in the mesoscale are generated in a short time (hours), even though these structures are missing from the initial state in the forecasts because of difficulty in obtaining and assimilating high-resolution observations. Thus the models are capable of generating the dynamically correct mesoscale structures and energy spectrum even without their initialization. This argues for further development and evaluation of mesoscale and cloud-scale NWP.

From an NWP perspective, spectra can not be verified in a deterministic manner because we do not have sufficient high-resolution observations. At the larger scales, verification of the forecast implies verification of the spectrum. At the mesoscale, structures forced by accurately forecast larger-scale structures, or by accurately specified external forcings, may benefit deterministic forecast accuracy. If deterministic forecasting of some mesoscale structures is not feasible, the spectral results support the argument that the energetics of these structures are generally consistent with observations, and upscale growth (energy cascade) may benefit determin-

istic forecasts of larger-scale structures. This result may be of particular importance when transitioning from parameterized to resolved deep convection—deterministic forecast of convective cells may be possible only on time scales of tens of minutes, but their net (larger-scale) effect on the forecasts should be energetically correct.

Forecast kinetic energy spectra can be used to address a number of issues that are critically important for advancing high-resolution NWP models. First, the choice and subsequent tuning of dissipation mechanisms in high-resolution models is not usually tied to quantitative evaluation of dynamical resolution in forecasts. Typically filters are tuned based on a qualitative assessment of the amount of noise in forecasts, or are tuned to maximize some verification measure. The latter approach is particularly problematic as NWP models are pushed to higher resolution where traditional verification measures will show decreased skill as models resolve increasingly finer-scale structures that are more inherently nondeterministic at NWP time scales. Second, the push to higher resolution is costly, and model efficiency must be of utmost concern in model formulation. For example, doubling the horizontal resolution of a model generally increases the computational cost of a model by a factor of 8. Furthermore, model resolutions are increased primarily to better resolve structures at the resolution limit, as opposed to better resolving already well-resolved structures. Thus, it is the ability of a model to resolve features at the highest wavenumbers representable on a grid that is of most importance, and an important measure of model efficiency must be resolving capability relative to computational cost. Thus spectra can be used not only to evaluate and tune dissipation formulations, but to discriminate more generally among model formulations.

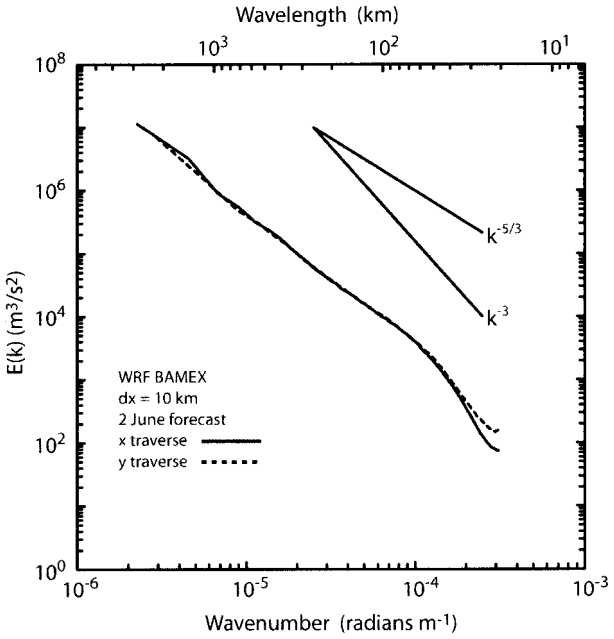


FIG. A1. Spectra from the 1 Jun 2003 BAMEX forecast using 10-km grid spacing. Spectra are computed using forecast grid lines that are nominally oriented west–east (x) and south–north (y).

## APPENDIX

### Computation of Spatial Spectra

The one-dimensional kinetic energy spectrum, based on a spectral decomposition of the velocity fields, represents a concise measure of energy as a function of length scale. In this appendix we consider a number of issues that arise in computing a one-dimensional KE spectrum on the limited-area domains characteristic of high-resolution NWP models.

The velocity fields are multidimensional, and multidimensional transforms are most often used for their decomposition. The approach typically employed to collapse results from a 3D or 2D transform to a single dimension is to integrate the energy density over shells in wavenumber space (see Errico 1985). The observational data to which we compare the model spectra are, however, not multidimensional; the Nastrom and Gage (1985) spectrum is computed using aircraft flight data that can be most accurately described as lying along lines in space. In order to simplify the comparison with observations, and to simplify the NWP forecast spectral computation, we have chosen to compute a 1D spectrum by averaging 1D spectral energy densities computed using 1D spectral decompositions of the velocity fields

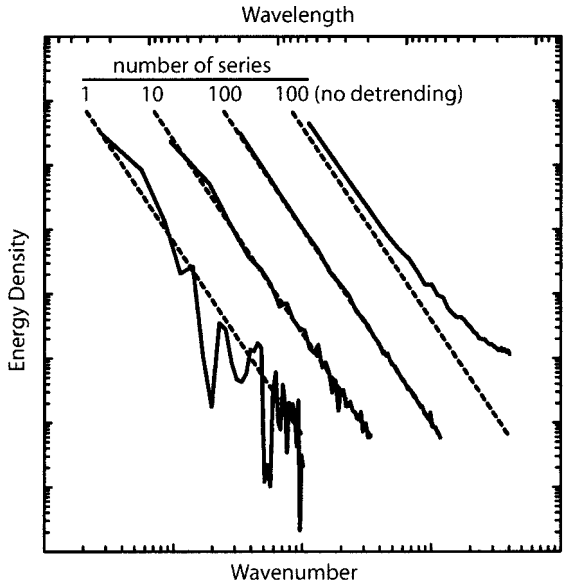


FIG. A2. Spectra computed using series of length L possessing a $k^{-3}$ dependence, truncated at 3/4 L. Random phase shifts are included in the individual Fourier components used to construct the series. The spectra are, from left to right, from a single series, averaged over 10 and then 100 series, and averaged over 100 series but with no detrending. The exact spectra are given by the dashed lines in each case.

along the horizontal coordinate axes of the model forecasts. We have found that it is adequate to compute the 1D spectra along the nominal east–west forecast grid direction; there is little difference between spectra computed using lines in the east–west direction, the north–south direction, or an average of the two directions. An example of the lack of directional dependence of the spectrum is shown in Fig. A1, where W–E, N–S, and W–E/N–S averaged spectra are plotted for the 1 June 2003 WRF BAMEX forecast.

The second and perhaps most obvious problem is the lack of periodic boundary conditions needed for the spectral decomposition in limited-area domains. The most common approach used to examine one-dimensional nonperiodic data is to remove the linear trend from the series, thereby rendering the data periodic (e.g., Errico 1985). While this renders the series periodic, there remains the problem that modes will be truncated by the domain boundaries and by the removal of the linear trend. In order to examine this issue, we have constructed discrete random periodic series, containing $N$ points and possessing a $k^{-3}$ power spectrum, and we have sampled $3N/4$ points in this series and computed its spectrum. The resulting truncated power spectra are shown in Fig. A2. An individual spectra will contain significant errors (and much erroneous noise) because of the series truncation, as shown by the leftmost spectra. Averaging over an increasingly larger sample of individual spectra will filter out the noise, as indicated by the middle two spectra using sample sizes of 10 and 100 individual spectral lines. The rightmost spectrum shows that when the linear trend is not removed, the turned-up tail of the spectrum indicates that strong aliasing of the truncated wavelengths will result in a relatively smooth and completely erroneous spectra. Not only is the behavior of the tail in error, the entire spectrum has too much energy.

## REFERENCES


Balmino, G., 1993: The spectra of the topography of the Earth, Venus and Mars. *Geophys. Res. Lett.,* **20,** 1063–1066.

Boer, G. J., and T. G. Shepherd, 1983: Large-scale two-dimensional turbulence in the atmosphere. *J. Atmos. Sci.,* **40,** 164–184.

Bryan, G. H., J. C. Wyngaard, and J. M. Fritsch, 2003: Resolution requirements for the simulation of deep moist convection. *Mon. Wea. Rev.,* **131,** 2394–2416.

Charney, J. G., 1971: Geostrophic turbulence. *J. Atmos. Sci.,* **28,** 1087–1095.

Cho, J. Y. N., R. Newell, and J. D. Barrick, 1999a: Horizontal wavenumber spectra of winds, temperature, and trace gases during the Pacific Exploratory Missions: 2. Gravity waves, quasi-two-dimensional turbulence, and vortical modes. *J. Geophys. Res.,* **104,** 16 297–16 308.

——, and Coauthors, 1999b: Horizontal wavenumber spectra of winds, temperature, and trace gases during the Pacific Exploratory Missions: 1. Climatology. *J. Geophys. Res.,* **104,** 5697–5716.

Davis, C., and Coauthors, 2004: The bow echo and MCV experiment: Observations and opportunities. *Bull. Amer. Meteor. Soc.,* **85,** 1075–1093.

Denis, B., J. Côté, and R. Laprise, 2002: Spectral decomposition of two-dimensional atmospheric fields on limited-area domains using the Discrete Cosine Transform (DCT). *Mon. Wea. Rev.,* **130,** 1812–1829.

Dewan, E. M., 1979: Stratospheric spectra resembling turbulence. *Science,* **402,** 832–835.

Done, J., C. Davis, and M. Weisman, 2004: The next generation of NWP: Explicit forecasts of convection using the Weather Research and Forecast (WRF) model. *Atmos. Sci. Lett.,* in press.

Dudhia, J., 1993: A nonhydrostatic version of the Penn State/NCAR Mesoscale Model: Validation tests and simulation of an Atlantic cyclone and cold front. *Mon. Wea. Rev.,* **121,** 1493–1513.

Errico, R. M., 1985: Spectra computed from a limited area grid. *Mon. Wea. Rev.,* **113,** 1554–1562.

Gage, K. S., 1979: Evidence for a $k^{-5/3}$ law inertial range in mesoscale two-dimensional turbulence. *J. Atmos. Sci.,* **36,** 1950–1954.

Hodur, R. M., 1997: The Naval Research Laboratory's Coupled Ocean/Atmosphere Mesoscale Prediction System (COAMPS). *Mon. Wea. Rev.,* **125,** 1414–1430.

Janjic, Z. I., 2003: A nonhydrostatic model based on a new approach. *Meteor. Atmos. Phys.,* **82,** 271–285.

Koshyk, J. N., and K. Hamilton, 2001: The horizontal kinetical energy spectrum and spectral budget simulated by a high-resolution troposphere–stratosphere–mesosphere GCM. *J. Atmos. Sci.,* **58,** 329–348.

Kraichnan, R. H., 1967: Inertial ranges in two-dimensional turbulence. *Phys. Fluids,* **10,** 1417–1423.

Laursen, L., and E. Eliasen, 1989: On the effects of the damping mechanisms in an atmospheric general circulation model. *Tellus,* **41A,** 385–400.

Lean, H. W., and P. A. Clark, 2003: The effects of changing resolution on mesoscale modelling of line convection and slantwise circulations in FASTEX IOP16. *Quart. J. Roy. Meteor. Soc.,* **129,** 2255–2278.

Lilly, D. K., 1969: Numerical simulation of two-dimensional turbulence. *Phys. Fluids,* **12** (Suppl. II), 240–249.

——, 1983: Stratified turbulence and the mesoscale variability of the atmosphere. *J. Atmos. Sci.,* **40,** 749–761.

——, and E. Peterson, 1983: Aircraft measurements of atmospheric energy spectra. *Tellus,* **35A,** 379–382.

——, G. Bassett, K. Droegemeier, and P. Bartello, 1998: Stratified turbulence in the atmospheric mesoscales. *Theor. Comput. Fluid Dyn.,* **11,** 139–153.

Lindborg, E., 1999: Can the atmospheric kinetic energy spectrum be explained by two-dimensional turbulence? *J. Fluid Mech.,* **388,** 259–288.

——, and J. Y. N. Cho, 2001: Horizontal velocity structure functions in the upper troposphere and lower stratosphere: 2. Theoretical considerations. *J. Geophys. Res.,* **106,** 10 233–10 242.

Michalakes, J., S. Chen, J. Dudhia, L. Hart, J. Klemp, J. Middlecoff, and W. Skamarock, 2001: Development of a next generation regional weather research and forecast model. *Developments in Teracomputing: Proceedings of the Ninth ECMWF Workshop on the Use of High Performance Computing in Meteorology,* W. Zwieflhofer and N. Kreitz, Eds., World Scientific, 269–276.

Nastrom, G. D., and K. S. Gage, 1985: A climatology of atmospheric wavenumber spectra of wind and temperature observed by commercial aircraft. *J. Atmos. Sci.,* **42,** 950–960.

Otte, M. J., and J. C. Wyngaard, 2001: Stably stratified interfacial-layer turbulence from large-eddy simulation. *J. Atmos. Sci.,* **58,** 3424–3442.

Skamarock, W. C., J. B. Klemp, and J. Dudhia, 2001: Prototypes for the WRF (Weather Research and Forecasting) model. Preprints, *Ninth Conf. on Mesoscale Processes,* Fort Lauderdale, FL, Amer. Meteor. Soc., J11–J15.

Snyder, C., W. C. Skamarock, and R. Rotunno, 1993: Frontal dynamics near and following frontal collapse. *J. Atmos. Sci.,* **50,** 3194–3212.

Vallis, G. K., G. J. Schutts, and M. E. B. Gray, 1997: Balanced mesoscale motion and stratified turbulence forced by convection. *Quart. J. Roy. Meteor. Soc.,* **123,** 1621–1652.

VanZandt, T. E., 1982: A universal spectrum of buoyancy in the atmosphere. *Geophys. Res. Lett.*, **9,** 575–578.

Vinnichenko, N. K., 1970: The kinetic energy spectrum in the free atmosphere—1 second to 5 years. *Tellus*, **22,** 158–166.

Wicker, L. J., and W. C. Skamarock, 2002: Time splitting methods for elastic models using forward time schemes. *Mon. Wea. Rev.*, **130,** 2088–2097.

Xue, M., D.-H. Wang, J.-D. Gao, K. Brewster, and K. K. Droegemeier, 2003: The Advanced Regional Prediction System (ARPS), storm-scale numerical weather prediction and data assimilation. *Meteor. Atmos. Phys.*, **82,** 139–170.

Yuan, L., and K. Hamilton, 1994: Equilibrium dynamics in a forced-dissipative f-plane shallow-water system. *J. Fluid Mech.*, **280,** 369–394.